16th World Conference on Earthquake, 16WCEE 2017

Santiago Chile, January 9th to 13th 2017

Paper N° 751

Registration Code: S-E1463181694

SIMULATION ANALYSIS OF COLLAPSE PROCESS OF 18-STORY HIGH-RISE STEEL BUILDING BASED ON THE SHAKING-TABLE TEST

Y. Suzuki[1], K. Suita[2], J. Kubota[3] , Y. Sawamoto[4] , N. Koshika[5] and M. Takahashi[6]

[1] *General Manager, Structural Research Department, Kobori Research Complex Inc., y-suzuki@kobori-takken.co.jp*
[2] *Professor, Department of Architecture and Architectural Engineering, Kyoto University, suita@archi.kyoto-u.ac.jp*
[3] *Chief Research Engineer, Building Structures Group, Kajima Technical Research Institute, jkubota@kajima.com*
[4] *Chief Research Engineer, Building Structures Group, Kajima Technical Research Institute, sawamoto@kajima.com*
[5] *Deputy Manager, Kobori Research Complex Inc., koshika@kobori-takken.co.jp*
[6] *General Manage, Building Structures Group, Kajima Technical Research Institute, motomi@kajima.com*

Abstract

The large scale shaking-table test of 18-story high-rise steel building was carried out at the E-Defense of Hyogo Earthquake Engineering Research Center. Through the study, analytical model could be developed to evaluate the collapse mechanism as the shaking-table test result for the first time.

Simulation analysis was conducted with the proposed hysteresis model considering the lower-flange fracture. The outcomes of the comparison between the simulation analysis and the shaking-table test results are summarized as follows:

1) Overall behavior of the test specimen

The maximum response of story drift angles of analytical results for all excitation levels were similar to the test results less than pSv300 and were slightly higher under the level of pSv300 to pSv420 excitation.

The maximum shear forces of analyses corresponded to the test results, and the degree of increase in shear force with changes in excitation level agreed well.

The time history of relative displacement of the 12th floor was represented well by the simulation analysis, except the residual deformation. The deterioration of shear force versus story drift angle was evaluated well, especially in the characteristic of reverse S-shaped hysteresis.

2) Progress of pre-collapse damage

Good correspondence with the test results was seen for the each stage of damage process, namely: yielding of the beam ends and column ends at the first floor, first occurrence of fracture of the lower flanges of the beam-ends at the second floor, spread of fracture to some beam-ends at the upper floors, fracture of the lower flanges of all the beam-ends at the lower floors, and large deformation of the lower floors.

3) Mechanism of the eventual collapse

The influence of the P-Δ effect became remarkable as the increase in the horizontal deformation, and further major deformation occurred after that. At the end, the enormous deformation occurred at lower five floors and the test specimen led to collapse. The analysis was well represented the test results above mentioned.

The validity of the simulation analysis model with the proposed deterioration hysteresis model was verified on the basis of above three points of view.

Keywords: high-rise steel building, collapse, fracture, simulation analysis, hysteresis model

1. Introduction

The importance of countermeasures for unexpected earthquakes was emphasized by the 2011 Great East Japan Earthquake. For the important roles played by high-rise buildings in urban areas as centers for everyday life and business, a large-scale shaking-table test was carried out to clarify the collapse process of a high-rise steel building ([3], Figure 1). This study's ultimate goal was to evaluate the collapse margin of various types of high-rise buildings. In this study, a method of analysis and an analytical model were first developed to enable evaluation of the shaking-table test results.

As for the collapse of a steel high-rise building, local buckling and fracture are regarded as the main deterioration factors in beams and columns. In the shaking-table test [3], the deterioration was seen with the lower flange fracture of the beams from small excitation levels and the sudden deterioration was seen in the columns at the excitation level leading to collapse.

In order to represent the deterioration of beams and columns, deterioration models (for example [4-8]) have been proposed. The models are assumed that the deterioration is moderate. Local buckling of the steel beams is an equivalent form of the moderate deterioration. Conversely, fracture macro models have also been proposed (for example [9]). However, they cannot exactly represent the behavior after fracture because the modeled resistance has no moment or a small constant moment.

The simulation analysis for the collapse test of the entire building model was carried out in [10-11], but one collapse test [10] depended on gradual deterioration of the local buckling and another test [11] was conducted with the small reduction model in which it was not possible to consider actual welding conditions etc.

Therefore, in the present study, the deterioration hysteresis model was proposed which can represent well the characteristics after lower flange fracture of the beam-ends. A simulation analysis of the shaking-table test, in which the fracture of the beam-ends greatly influenced the behavior, was conducted. Simulation analysis was compared with those of the shaking-table test. Focus was placed on the overall behavior of the test specimen in the elastic domain and in the weak/strong nonlinearity domains, the progress of pre-collapse damage, and the mechanism behind eventual collapse. Through these comparisons, the validity of the simulation analysis model with the proposed deterioration hysteresis model was verified.

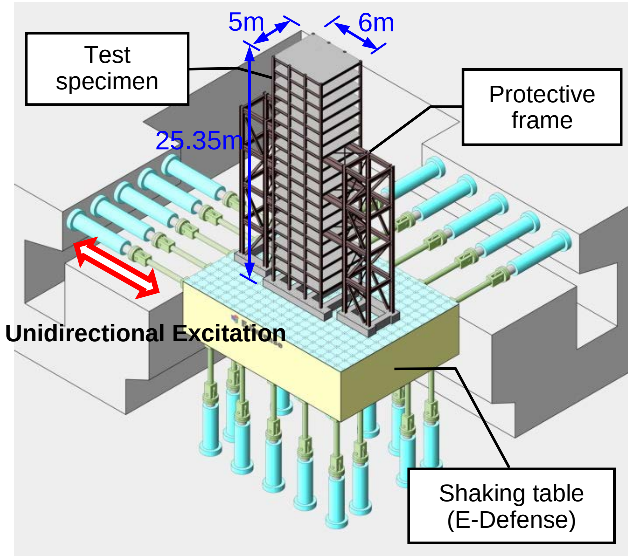

Fig. 1 – Shaking-table test at E-Defense

2. Outline of Shaking Table Test

2.1 Basics of the test specimen

(1) Test specimen frame and beam/column cross section

The test specimen was produced at a 1/3 scale with 18 stories (Fig. 2). It was designed as a moment resisting frame and its floor dimensions were 6 m (2 m; three bays) in the input direction and 5 m (5 m; one bay) in the orthogonal direction, and the total height was 25.35 m. The story heights were 1.70 m (first floor) and 1.35 m (2nd–18th floors). The slenderness ratio was approximately 4.2 (= 25.35/6).

The beam/column cross sections are shown in Fig. 2. The beams of the orthogonal frame were the G1 type (H-250 × 125 × 6 × 9, SM490A), and the footing beams were reinforced concrete with steel beams.

(2) Slabs and additional weights

The floors were of the deck slab type with a thickness of 50 mm. The design standard strength of the slab concrete was 21 N/mm^2, and stud bolt placements were based on that of structures built in the 1980s–1990s.

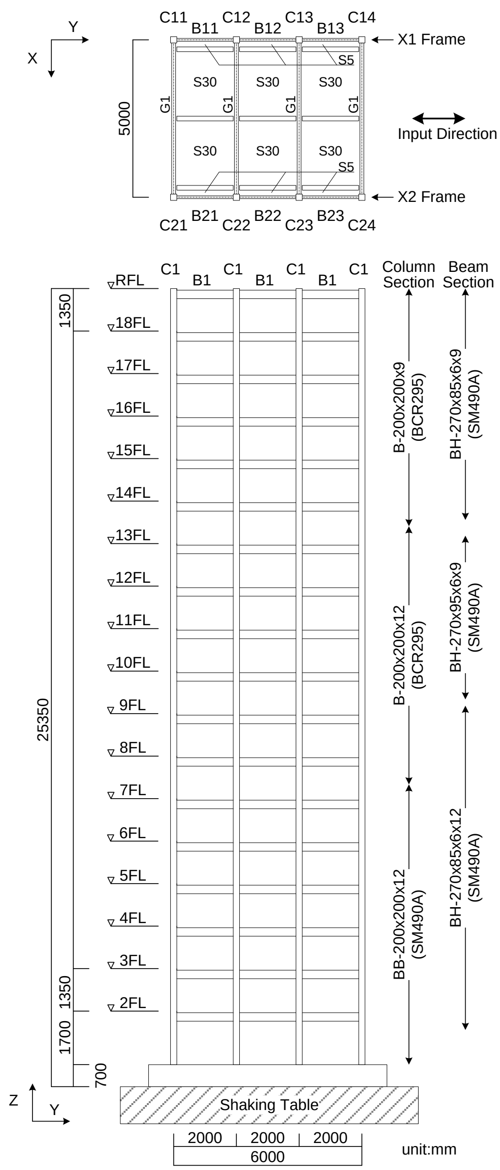

Fig. 2 – Test specimen floor plan and elevation

Table 1 – Tensile test results

	Material	Part	t mm	Test Piece ※1	Note	upper yield stress N/mm^2	lower yield stress N/mm^2	tensile strength N/mm^2	elongation %	yield ratio %	reduction of area %
Column	SM490A	C1	12	1A	BB-1	384	374	523	27	73	71
					BB-2	382	364	524	28	73	71
					BB-3	384	360	521	28	74	73
	BCR295	C1	12	1A	2C-1	437	420	467	20	94	-
					2C-2	431	425	467	21	92	-
					2C-3	435	423	468	19	93	-
	BCR295	C1	9	1A	3C-1	438	423	457	23	96	-
					3C-2	445	418	458	26	97	-
					3C-3	430	405	455	19	95	-
Beam	SM490A	B1	12	1A	B1-1	393	372	540	28	73	60
					B1-2	397	364	541	25	73	58
					B1-3	392	364	538	26	73	-
	SM490A	B1	9	1A	B1-4	385	368	540	25	71	-
					B1-5	385	368	540	25	71	-
					B1-6	383	365	539	28	71	-
					B1-7	384	364	539	27	71	-
					B1-8	384	368	538	25	71	-
					B1-9	387	369	537	26	72	-
	SM490A	B1	6	1A	B1-10	476	445	572	19	83	56
					B1-11	478	449	575	20	83	56
					B1-12	475	438	568	20	84	56

※1:Japanese industrial standards(JIS Z 2201)

2.2 Input excitation

The simulated earthquake input used in the test was based on long-period ground motion predicted from mega-thrust fault earthquakes expected to occur in the Nankai Trough. The velocity time histories and spectra are shown in Fig. 3 and Fig. 4. In line with the law of similarity for the reduced scale of the test specimen, the time period of simulated earthquake excitation was shortened to produce the excitation waves. In each excitation, the amplitude was coordinated using the magnification factor on the basis of the excitation wave. The excitation schedule is shown in Table 2.

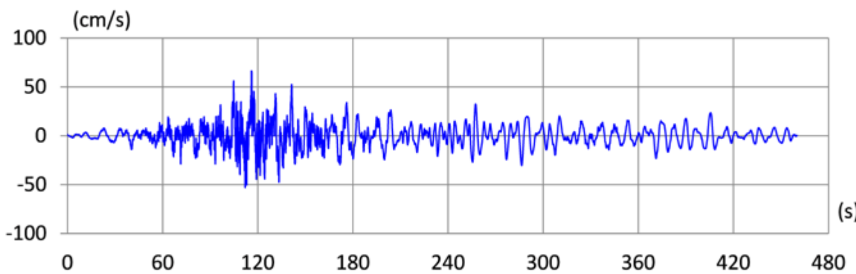

Fig. 3 – Velocity time history of the simulated long-period earthquake ground motion

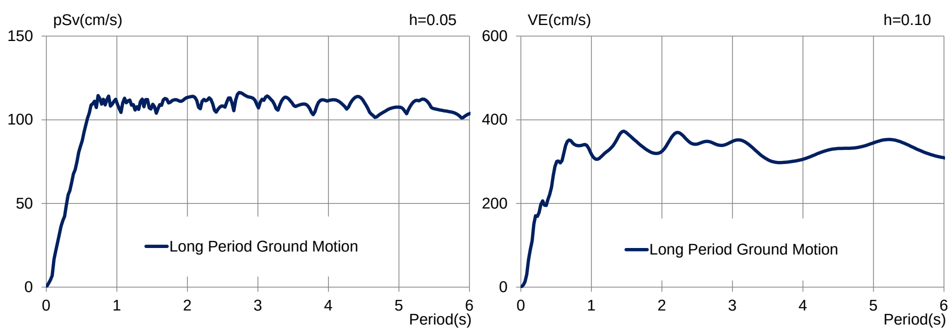

Fig. 4 – Pseudo velocity response spectrum and energy spectrum of the ground motion of the simulated long-period earthquake

Table 2 – Shaking-table test schedule

Excitation Level		Legends	Remarks
pSv16cm/s	0.15		Design
pSv40cm/s	0.36	pSv40	Design(Elastic)
pSv81cm/s	0.74	pSv81	Design(Plastic)
pSv110cm/s	1.00	pSv110-1	Average Level*1
pSv110cm/s	1.00	pSv110-2	Average Level*1
pSv180cm/s	1.64	pSv180-1	Maximum Level*1
pSv180cm/s	1.64	pSv180-2	Maximum Level*1
pSv220cm/s	2.00	pSv220	over Maximum Level*1
pSv250cm/s	2.27	pSv250	over Maximum Level*1
pSv300cm/s	2.73	pSv300	over Maximum Level*1
pSv340cm/s	3.10	pSv340-1	over Maximum Level*1
pSv340cm/s	3.10	pSv340-2	over Maximum Level*1
pSv420cm/s	3.82	pSv420-1	over Maximum Level*1
pSv420cm/s	3.82	pSv420-2	over Maximum Level*1

*1: Long Period Ground Motion at Aichi Pref. w hen Nankai-Trough Eartuquake

3. Simulation Analysis

3.1 Details of analysis

The details of the study's simulation analysis are described below.

1) A three-dimensional element-based frame model was used for the analysis. Beams and columns were modeled by beam-elements, and connection panels were modeled by pure shear panel models.

2) Axial, bending and shear deformation were considered for the columns, bending and shear deformation for the beams, and shear deformation for the panels. The elasto-plastic properties of the axial and bending deformation of the columns, bending deformation of the beams and shear deformation of the panels, were considered.

3) Floor slabs contributed to the beam stiffness with a stiffness increase factor of 1.2.

4) The elasto-plastic properties of the element model were set on a bi-linear basis, and the average of the material test results shown in Table 1 was used as the yield strength.

The column modeling method was based on the theory of plasticity, which allowed consideration of the correlation between the bending moment and axial force (Fig. 5). Ziegler's modification of Prager's hardening rule [12] was adopted for the hardening rule. Plastic stiffness was assumed to be 1% of the elastic stiffness in the axial force / axial deformation relationship and in the bending moment / rotation angle relationship.

The elasto-plastic characteristic of the shear panel was also considered. Plastic stiffness was assumed to be 1% of the elastic stiffness.

These columns and panels had normal-type hysteresis without deterioration.

5) Beams were modeled by a multi-component parallel model [13]. Any strength increase contributed by floor slabs was not considered. Hysteresis model for the beam ends was improved to a deterioration type in consideration of the lower-flange fracture (Fig. 6).

6) The P-Δ effect was considered with the additional shear force corresponding to the story drift (Fig. 7).

7) It was assumed that each floor was rigid and the lower ends of first-floor columns were fixed to the shaking table.

8) Weights of 211 kN were concentrated at the center of gravity of each floor.

9) The excitation wave was applied continually in line with the test schedule.

10) The damping ratio was set to 0.8% for the first mode and 0.2% for the second mode with reference to the test results and the simulation. The observed damping in the test was very small compared with actual tall buildings.

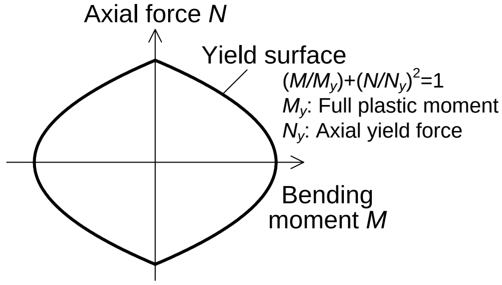

Fig. 5 – Axial force – bending moment relationship and yield surface

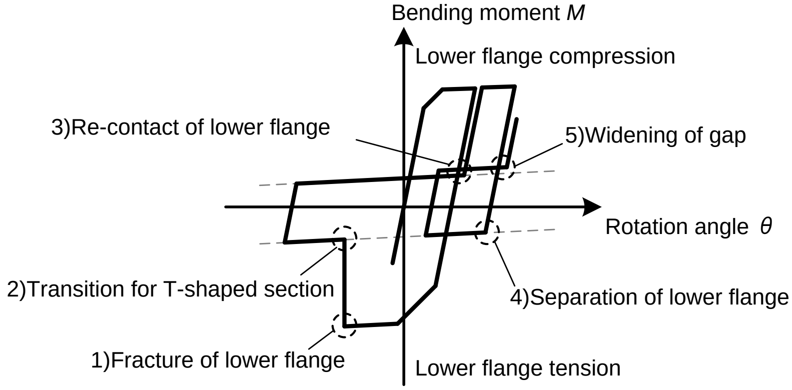

Fig. 6 – Hysteresis model for beam moment – rotation angle relationship in consideration of the lower-flange fracture

3.2 Deterioration hysteresis model for the beam ends with consideration of fracture

Beam elements underwent repeated plastic deformation in the shaking-table test, and eventually beam-end lower-flange fracture was assumed. A deterioration-type hysteresis model was used to represent this event. The characteristics were as follows:

1) As shown by a Tri-linear-type model with an H-shaped cross section, the resisting moment suddenly decreased after lower-flange fracture.

2) After such a fracture, 1/10 of the pre-fracture moment was assumed in consideration of the T-shaped cross section in a lower flange fracture.

3) The fractured flange was turned to the compression and reached the previous maximum deformation, the fractured flange touch again. The characteristic of an H-shaped cross section revived.

4) If the fractured flange was turned to the tension, the characteristic form changed to a T-shaped cross section because of the fractured flange separation.

5) When the fractured flange was turned to the compression and deformation progressed further, plastic deformation remained in the flange on the compression, and the point at which the fractured flange re-contacted became large.

The timing of the lower-flange fracture had to be decided. A performance curve obtained from a previous experimental study ([14], Eq. (1), Figure 8) was adopted. Miner's rule was considered to apply here, and damage D was added at every half cycle (Eq.(2)) in line with the plastic deformation capacity based on the performance curve. N_{fi} represented the number of cycles before beam-column connections accumulated plastic deformations and fractured. Coefficients β were evaluated using constant amplitude cyclic tests. β was a coefficient of the gradient in Figure 8. The coefficient C was decided to be 4.9 for the beams of lower floors and to be 5.7 for higher floors by trial and error. When damage D reached 1.0, fracture was deemed to occur.

$$N_{fi} = (C/\mu_i)^{1/\beta}, \ \beta = 1/3 \tag{1}$$

$$D = \sum 0.5 / N_{fi} \tag{2}$$

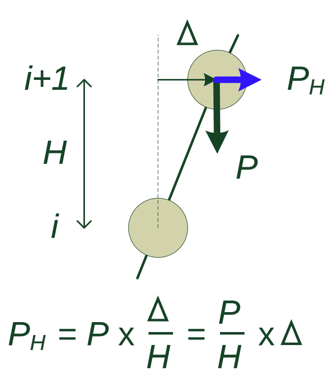

Fig. 7 – P-Δ effect incorporation

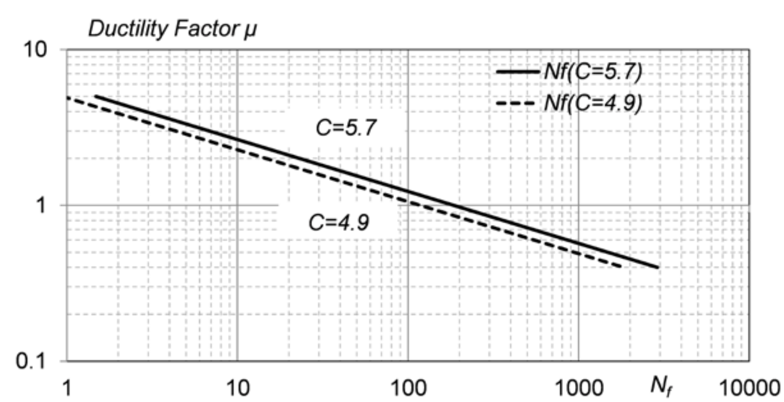

Fig. 8 – Cyclic deformation performance curve

3.3 Simulation analysis results

The analysis results and the corresponding test results are outlined below.

(1) Maximum response distribution (Fig. 9)

(a) Story drift angle: At an excitation level of pSv220, the analysis results corresponded closely with the test results. At pSv300, the analysis results were slightly higher. At pSv340-1, the analysis results were quite similar to the maximum and distribution shapes seen in the test results. At pSv420-1, although deformation concentration in the lower stories was taken into account, the maximum response deformation from the analysis was greater than for the test results.

(b) Story shear force: At an excitation level of pSv220, the analysis results varied with the combination of the first and second modal vibrations, but generally corresponded to values seen in the experiment. From pSv300 upward, the analysis clearly showed that the story shear force did not reach the expected higher level despite the large input.

(2) Time history of 12th-floor relative displacement (Fig. 10)

At an excitation level of pSv300, the analysis results corresponded closely to the test results. At pSv340-1, until the maximum deformation response at around 90 s, the analysis results corresponded closely with the test results. However, the analysis results did not represent the subsequent vibration well. From pSv420-1 upward, the analysis results tended to suggest higher residual deformation than the test results but the analysis results represented the extention of the vibration period of the test specimen. At pSv420-3, the analysis results showed a rapid increase after 60 s. The behavior was similar with the test result.

(3) Relationships between the shear force and drift angle of the story (Fig. 11)

At an excitation level of pSv220, deterioration of the shear force/drift angle relationship began. This deterioration became significant at pSv300 and progressed further at pSv340-1. The hysteresis exhibited the reverse-S-shape as observed in the test results. But the maximum shear force in the analysis was slightly smaller than that in the test results.

(4) Relationships between beam moment and rotation angle (Fig. 12)

At an excitation level of pSv220, the deterioration of the beam moment-rotation angle relationship began because of the fracture, and post-fracture hysteresis deterioration was observed. After the lower-flange fracture, the return of stiffness and capacity and the expansion of the re-contact point (gap) on the lower flange compression side were similar to those observed in the test results.

(5) Component damage (Fig. 13)

At an excitation level of pSv220, the beams connected to outer columns on the second and third floors fractured first. At pSv300, beam fracture was seen on the upper floors, and all beam ends on the second and third floors fractured. The number of fracture points increased at pSv340-1. All beam ends from the second to the sixth floors fractured at pSv420-3, which was the final excitation, and fracture points were seen from the 12th to the 15th floors. Damage at each excitation level in the analysis corresponded to that in the test results.

(6) Relationships between the story shear force and drift angle up to collapse (Fig. 14)

The negative stiffness that showed the P-Δ effect is shown in the dotted gray lines in the figure as a guide. The shear force was generally quite small. In addition, the residual deformation at pSv340-2 and pSv420-1 was large. However, there was good correspondence with the test for the progress of the deformation and the hysteresis characteristics at pSv420-2 and pSv420-3.

The above observations indicated that the analysis produced results of the behavior of the test specimen at pSv110-1 when the specimen was in the weak nonlinearity domain, at pSv220 when the beam ends fractured and deterioration began, at pSv300 when the deterioration progressed, and from pSv340-1 to pSv420-3 when the test specimen exceeded the safety limit. It was also clear that the analysis could be used to successfully determine the mechanism behind the structure's eventual collapse.

4. Conclusions

This study's ultimate goal was to evaluate the collapse margin of various types of high-rise buildings. In this study, a method of analysis and an analytical model were first developed to enable evaluation of the shaking-table test results.

Simulation analysis was conducted with the proposed hysteresis model considering the lower-flange fracture of the beam-end using a tri-linear approach. A plastic deformation performance curve obtained from previous laboratory testing was adopted for considering the conditions when the fractures occurred, and a performance curve coefficient corresponding to the shaking-table test results was estimated. Miner's rule was applied for considering the influence from the plasticity amplitude history. In the analysis, it was assumed that damping was very small, corresponding to the test results.

The outcomes of the comparison between the simulation analysis results and the shaking-table test results are summarized as follows:

1) Overall behavior of the test specimen

The maximum response of story drift angles of analytical results for all excitation levels were similar to the test results less than pSv300 and were slightly higher under the level of pSv300 to pSv420 excitation.

The maximum shear forces of analyses corresponded to the test results, and the degree of increase in shear force with changes in excitation level agreed well.

The time history of relative displacement of the 12th floor was represented well by the simulation analysis, except the residual deformation. The deterioration of shear force versus story drift angle was evaluated well, especially in the characteristic of reverse S-shaped hysteresis.

2) Progress of pre-collapse damage

Good correspondence with the test results was seen for the each stage of damage process, namely: yielding of the beam ends and column ends at the first floor, first occurrence of fracture of the lower flanges of the beam-ends at the second floor, spread of fracture to some beam-ends at the upper floors, fracture of the lower flanges of all the beam-ends at the lower floors, and large deformation of the lower floors.

3) Mechanism of the eventual collapse

The influence of the P-Δ effect became remarkable as the increase in the horizontal deformation, and further major deformation occurred after that. At the end, the enormous deformation occurred at lower five floors and the test specimen led to collapse. The analysis was well represented the test results above mentioned.

The validity of the simulation analysis model with the proposed deterioration hysteresis model was verified on the basis of above three points of view.

The validity of the simulation analysis model with the proposed deterioration hysteresis model was verified on the basis of above three points of view.

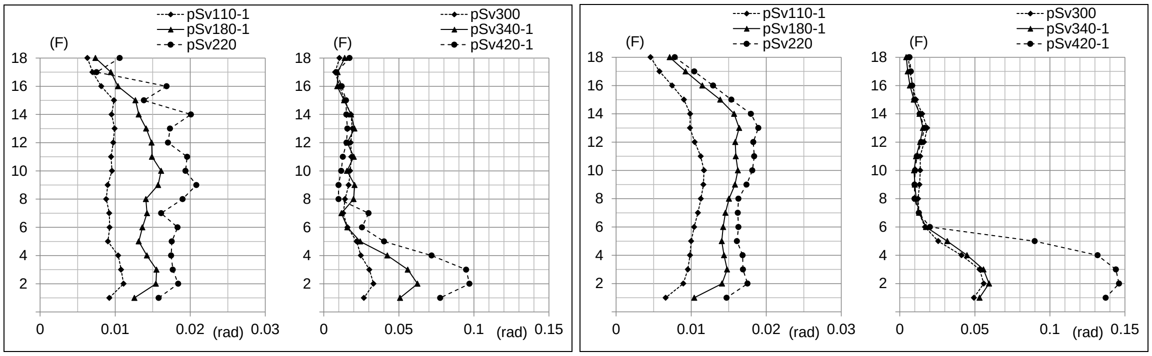

(a)Test results (b)Analysis

(1) Story drift angle

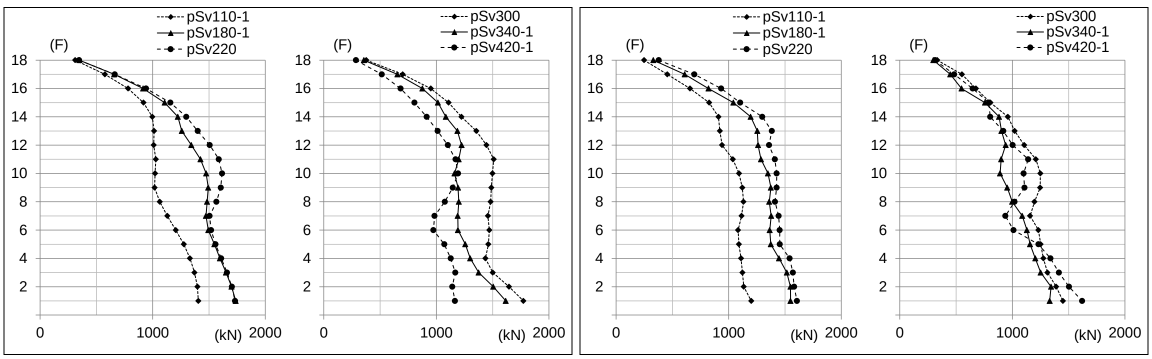

(a)Test results (b)Analysis

(2) Story shear force

Fig.9 – Maximum response value distributions (analysis)

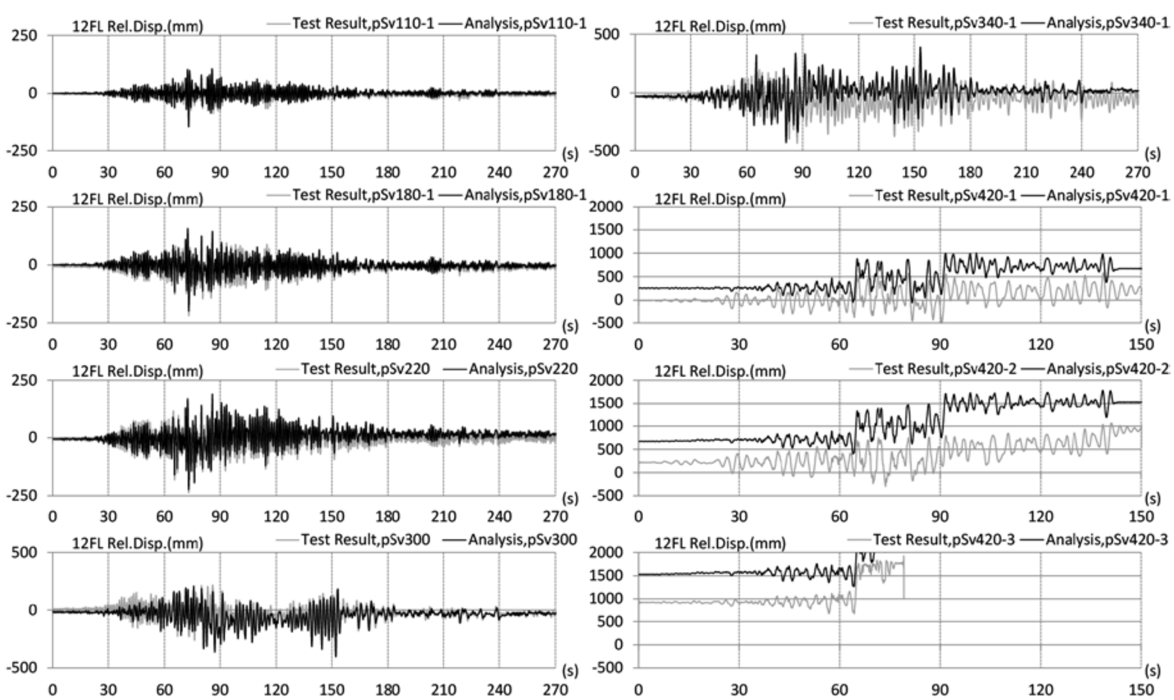

Fig. 10 – Time history of 12th-floor relative displacement (analysis)

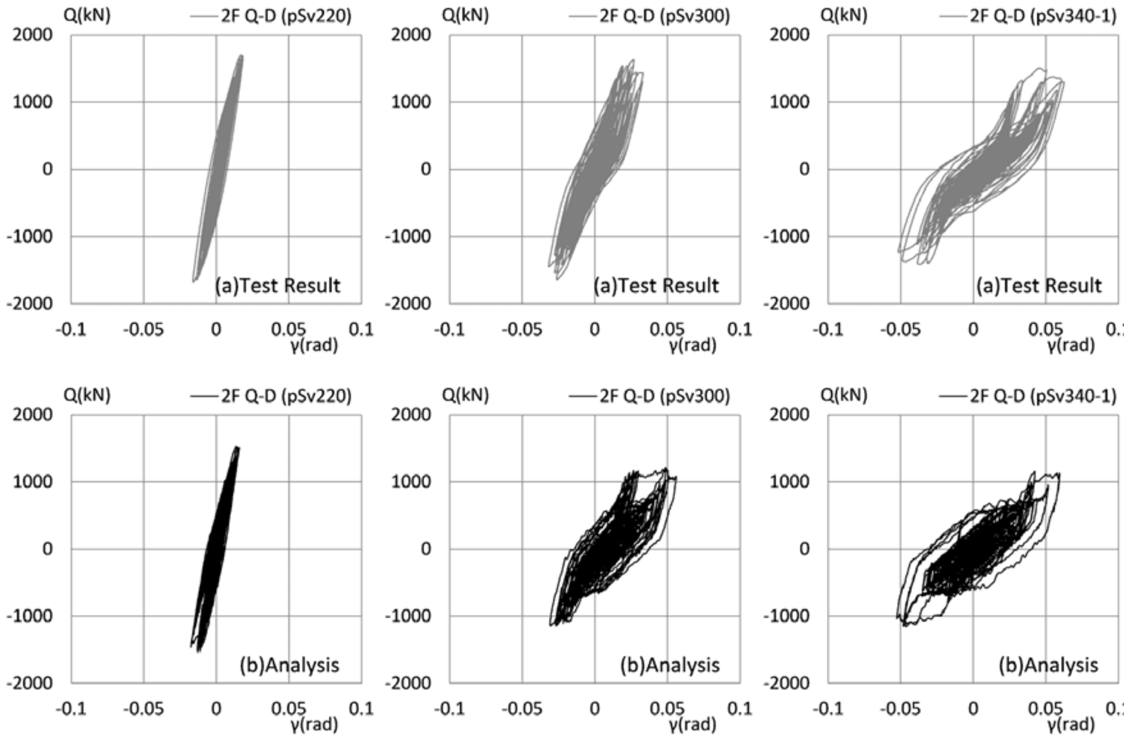

Fig. 11 – Relationships between story shear force and drift angle (second floor)

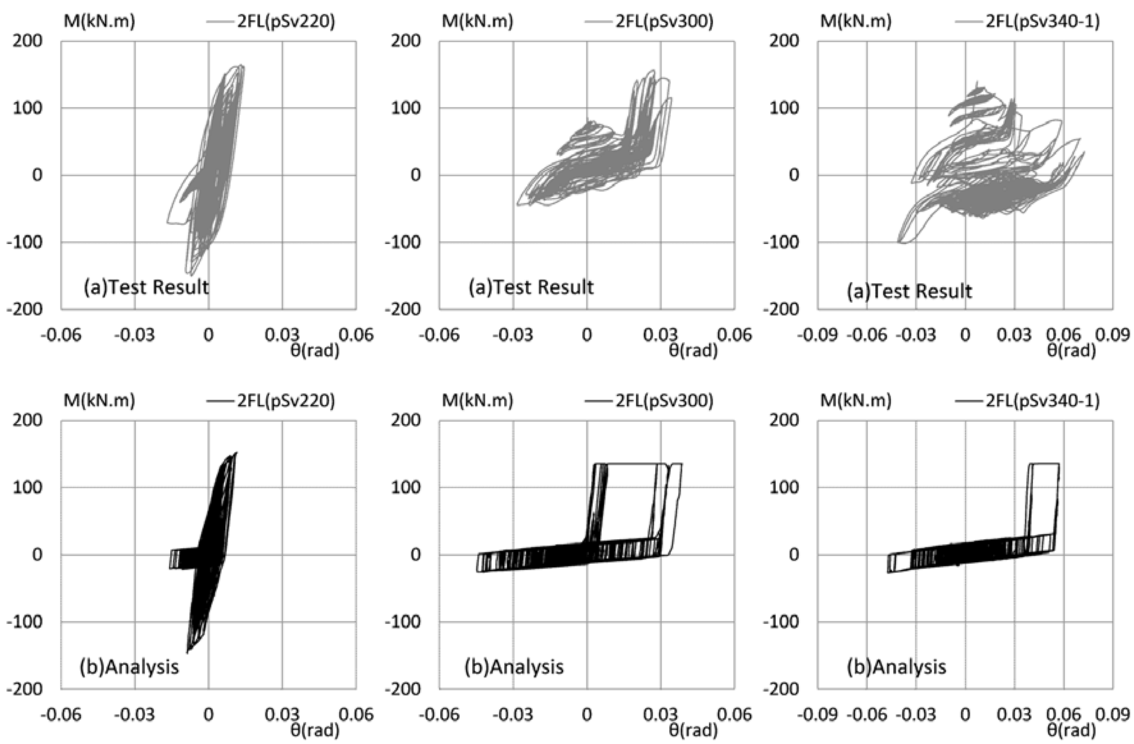

Fig. 12 – Beam M-θ relationships (second-floor B21 outer end)

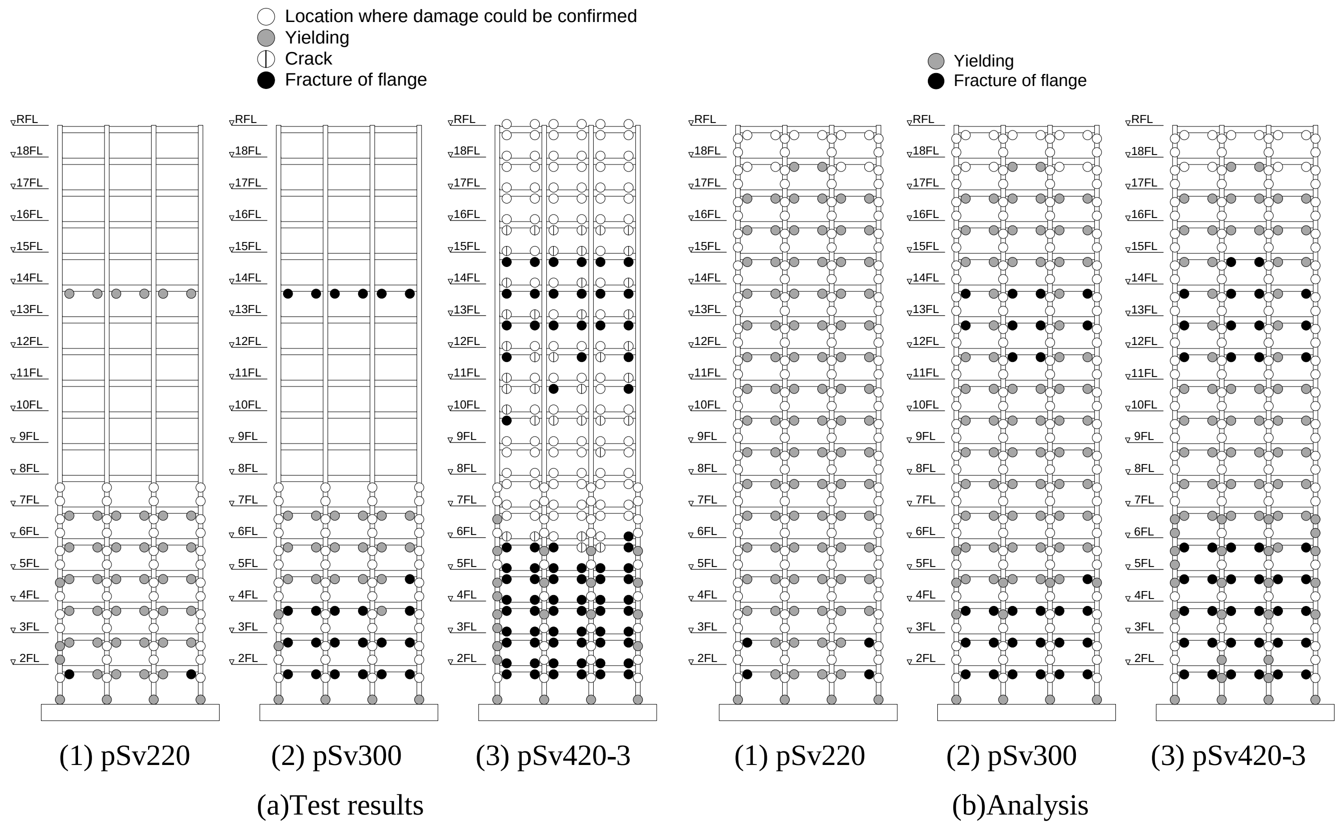

Fig. 13 – Beam and column damage

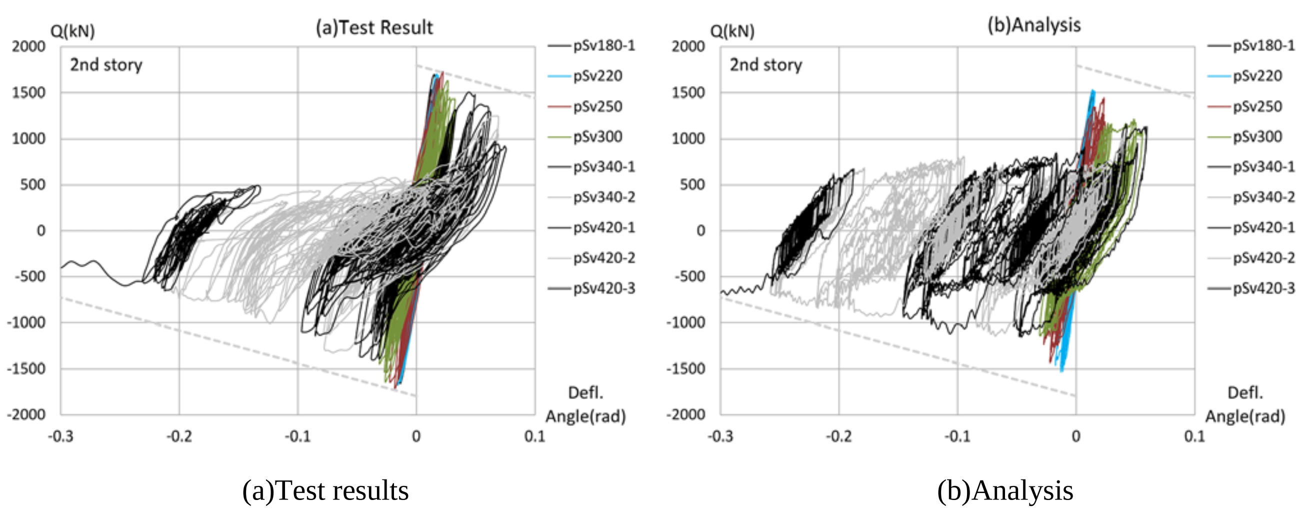

Fig. 14 – Relationships between story shear force and drift angle up to collapse (second floor)

5. Acknowledgements

The study was conducted as part of the research sponsored by Japan's Ministry of Education, Culture, Sports, Science and Technology under the title (ii) Maintenance and Recovery of Functionality in Urban Infrastructure, which is a sub-project of the Special Project for Reducing Vulnerability in Urban Mega Earthquake Disasters. The authors are grateful to all those who are contributed to and participated in the project. Particular thanks go to Associate Prof. Yuji Koetaka of Kyoto University, to Associate Prof. Jun Iyama of The University of Tokyo and to Associate Prof. Takuya Nagae of Nagoya University, for their assistance.

6. References

[1] Nakashima M, Suita K, Takahashi M, Nishiyama M, Katsumata H, Kajimawa K, Koshika N. Overview of 'Quantification of collapse margin of high-rise buildings' Quantification of collapse margin of steel high-rise buildings (Part 1). Summaries of Technical Papers from the Annual Meeting of the Architectural Institute of Japan 2013; 967 – 968 (in Japanese).

[2] Nakashima M. Roles of large structural testing for the advance of earthquake engineering. Proceedings of the 14th World Conference on Earthquake Engineering, Beijing, China, 2008; K009.

[3] Kubota J, Suita K, Kiyokawa T, Suzuki Y, Sawamoto Y, Koshika N, Takahashi M. A large-scale shaking table test of an 18-story high-rise steel building using the expected ground motion of the predicted Nankai Trough Earthquake. Earthquake Engineering and Structural Dynamics (submitted).

[4] Ibarra LF, Medina RA, Krawinkler H. Hysteretic models that incorporate strength and stiffness deterioration. Earthquake Engineering and Structural Dynamics, Volume 34, October 2005; 1489 – 1511

[5] Lignos DG, Krawinkler H. A database in support of modeling of component deterioration for collapse prediction of steel frame structures. Proceedings of Structural Engineering Research Frontiers, ASCE, 2007

[6] Tada M, Ohsaki M, Yamada S, Motoyui S, Kasai K. E-Defense tests on full-scale steel buildings Part3– Analytical simulation of collapse. Proceedings of Structural Engineering Research Frontiers, ASCE,2007

[7] Kato B, Akiyama H. The ultimate strength of the steel beam-column(Part 4). Journal of Structural and Construction Engineering, Architectural Institute of Japan, 1968, 151, 15 – 20 (in Japanese).

[8] Sivaselvan MV, Reinhorn AR. Hysteretic models for deteriorating inelastic structures. Journal of Engineering Mechanics, ASCE, June 2000, 633 – 640.

[9] Lavan O, Sivaselvan MV, Reinhorn AM, Dargush GM. Progressive collapse analysis through strength degradation and fracture in the mixed lagrangian framework. Proceedings of the 14th World Conference on Earthquake Engineering, Beijing, China, 2008.

[10] Lignos DG, Krawinkler H, Whittaker AS. Prediction and validation of sidesway collapse of two scale models of a 4-story steel moment frame. Journal of Earthquake Engineering and Structural Dynamics 2011, 40:807-825

[11] Lignos DG, Hikino T, Matsuoka U, Nakashima M. Collapse assessment of steel moment frames based on E-Defense full-scale shake table collapse tests, Journal of Structural Engineering, ASCE, June 2013, 120 – 132.

[12] Ziegler H. A modification of Prager's hardening rule. Applied Mathematics, Vol.17, No.1, 1959; 55 – 65

[13] Clough RW, Benuska KL, Wilson EL. Inelastic earthquake response of tall buildings. Proceedings of the 3rd World Conference on Earthquake Engineering, 1965; 68 – 89

[14] Narihara H, Yasuda S, Hasegawa T, Yamada S. Study on safety assessment methods for super-high-rise steel buildings against long-period earthquake ground motion (Part 20 Evaluation of low-cycle fatigue damage for steel beams at welded ends), Summaries of Technical Papers from the Annual Meeting of the Architectural Institute of Japan 2013; 1087 – 1088 (in Japanese).